Iron contamination in silicon solar cell production environments

Malcolm D. Abbott[1], Dmitry Poplavskyy[2], Giuseppe Scardera[2], Daniel Inns[2], Francesco Lemmi[2], Keith R. McIntosh[1] and Simeon C. Baker-Finch[1]

[1] PV Lighthouse, Coledale, Australia
[2] DuPont Silicon Valley Technology Center, Sunnyvale, U.S.A.

***Abstract* — The fundamental mechanisms of iron impurities in silicon have been thoroughly studied and are well explained in the literature. Of interest to solar cell manufacturers is to understand how these mechanisms manifest in a production environment and, more importantly, how to quickly diagnose and mitigate iron contamination as it occurs. This paper presents examples of iron contamination using p-type CZ wafers processed in production-style environments. The impact of iron on the IV performance of industrial screen printed solar cells is presented, including the time dependence of these effects and how they manifest in the various characterisation techniques that are typically used to diagnose solar cell performance. Examples are given of potential sources of iron contamination and the impact of subsequent processing on the redistribution of those contaminants. The paper demonstrates that iron contamination can occur in a variety of ways, can spread quickly and is severely detrimental to solar cell efficiency. Additionally, it is shown that the fundamental properties of iron in silicon can be used to quickly identify the root cause of contamination in a production environment.**

***Index Terms* — contamination, defects, recombination, manufacturing, photovoltaic cells, silicon.**

I. Introduction

Iron contamination can severely degrade the electrical performance of p-type silicon solar cells [1], [2]. Silicon solidified from lower-grade feedstock – or in an inevitably impure crucible – often contains a significant concentration of iron [3]. Typically, the detrimental impact of this contamination is mitigated during solar cell processing using techniques such as gettering. On the other hand, mono-crystalline substrates such as those fabricated from high-quality poly-Si using the Czochralski (CZ) method typically do not contain intrinsic iron in levels that are significant enough to impact on the device performance. However, such substrates can still be severely impacted by extrinsic sources of iron contamination that exist at many stages of the solar cell production process. The resultant degradation of the bulk lifetime can have a particularly negative impact in higher efficiency cell architectures, in which the suppression of surface recombination leads to a strong dependence of efficiency on bulk lifetime.

Iron is contained in much of the equipment that is used to produce solar cells; we show that care must be taken to avoid its transfer from the tools and chemicals onto the surface of the wafers from where it can make its way into the bulk of the solar cells. This is a crucial consideration in the search for ever-cheaper manufacturing tools and techniques. The semiconductor industry went to great lengths to improve tools, cleaning and handling procedures of wafers to minimise these sources of contamination. An excellent overview of process induced contamination was presented by Istratov [4] who pointed out that much of the information regarding specific tool contamination is often kept secret by the manufacturers and, in any case, is not necessarily relevant given the rapid change in these tools.

It is critically important that solar cell manufacturers fully appreciate the extrinsic sources of iron that can be easily introduced during the cell manufacturing process. Furthermore, manufacturers should be equipped with appropriate techniques to characterise, analyse and resolve the device-level impacts of this contamination. This paper identifies sources and identification techniques via the analysis of a series of examples of unintentional iron contamination that occurred on DuPont's 10 MW pilot line facility in California, which uses all standard production tools. The impact of iron contamination on finished solar cells fabricated on p-type CZ substrates is assessed and the transient nature of this iron-induced efficiency reduction is discussed, particularly in the context of flash testers which do not necessarily detect the full impact of the contamination.

II. Background

The fundamental properties of iron in silicon have been well studied [5], [6]. Here we present a brief overview of the key characteristics within the context of solar cell manufacturing. As we will show in the experimental section later in this paper, these fundamental properties describe very well the basic mechanisms behind the nature of extrinsic iron contamination and its impact on solar cell efficiency.

Iron is extremely mobile in silicon wafers, particularly at the temperatures typically used to produce standard screen-printed cells. It has been shown that the results of numerous studies into the temperature dependent diffusivity of iron can be fit by the linear relationship [6],

$$D(Fe_i) = (1.0^{+0.8}_{-0.4}) \times 10^{-3} \exp\left(\frac{0.67}{k_B T}\right) \qquad (1)$$

By making some simple assumptions, this equation can be used to estimate the extent to which iron will spread both laterally out of a point source and into the bulk of a silicon wafer. To provide a worst case estimate of the depth of silicon affected we have assumed that the source of iron on the surface does not deplete and that its diffusion into silicon is

therefore described by the error function. Iron will cause a significant reduction in bulk lifetime in p-type wafers for concentrations greater than 10^9 cm^{-3} and as such for each condition we have plotted the depth of silicon that is predicted to contain at least this much iron. This calculation was performed for three different surface concentrations and two thermal processes that are representative of those used in standard screen-printed cell production. For a typical $POCl_3$ emitter diffusion (Fig. 1. top) iron is predicted to potentially diffuse through a depth of silicon equivalent to multiple wafers. Even the short high temperature step encountered during paste firing (Fig. 1. bottom) could be expected to drive iron many micrometers into the wafer bulk.

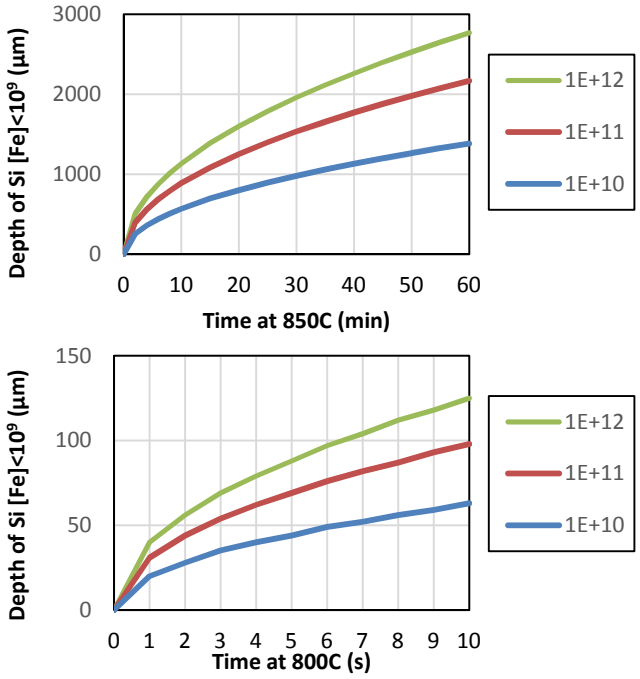

Fig. 1. Depth of [Fe] diffusion that results in a concentration less than 10^9 cm^{-3} shown for various surface concentrations of Fe.

Once in the bulk of a p-type silicon wafer, mobile iron exists either interstitially (Fe_i) or as an iron-boron pair (FeB) [5]. A summary of the properties of both types of this Shockley-Read-Hall (SRH) defect is shown in Table I. It should be noted that the ratio of capture cross sections (σ_n/σ_p) is vastly different between the two defects. The high ratio for Fe_i results in a very strong injection level dependence of the recombination introduced by this defect in p-type silicon.

TABLE I
SRH RECOMBINATION PARAMETERS FOR FEI AND FEB

Defect	E_t-E_i (eV)	σ_n (cm^2)	σ_p (cm^2)	σ_n/σ_p	Ref
Fe_i	0.183	4.0E-14	7.0E-17	571	[6]
FeB	-0.302	5.0E-15	3.0E-15	1.67	[7]

Mobile iron atoms in a silicon wafer are able to rapidly change between these two forms, particularly in response to strong illumination. At room temperature in the dark, all of the mobile iron will bond with boron atoms forming iron-boron pairs, FeB. Application of light (e.g. for 10 seconds at 1-Sun) will result in the breaking of these bonds and the formation of interstitial iron, Fe_i. In the dark, the reformation of the FeB pairs is somewhat slower and is described by a characteristic association time constant shown below [8].

$$\tau_{assoc} = 5.0 \times 10^5 \frac{T}{N_A} \exp\left(\frac{0.66}{k_B T}\right) \qquad (2)$$

Applying this equation to a typical 2 Ω·cm wafer (similar to those used later in this paper) predicts an association time constant of 52 minutes. As we will show in the experimental section, the recovery of an iron contaminated solar cell IV properties after a light soak can be very well described by Equation 2.

By using illumination to toggle between the two forms of iron it is possible to quickly detect the presence of iron contamination within silicon wafers in which the surfaces are fairly well passivated. Furthermore it has been shown that by further analysing these two curves it is possible to extract the actual concentration of mobile Fe in the bulk [5].

It is important to note that there exist other forms of contamination in the bulk of silicon wafers that respond to illumination. The most common in commercial grade CZ silicon is the so called light-induced degradation effect in which illumination results in the formation of boron-oxygen pairs. The possibility of other types of defects changing the bulk lifetime with illumination means that one should be careful when attempting to diagnose iron as the cause of contamination. The other properties of iron should be used to more clearly identify it. In particular the unique cross-over point at an excess minority carrier density of 10^{14} cm^{-3} as well as the reformation of FeB pairs in the dark with a well-known time constant. There is an entire periodic table of possibilities when it comes to contamination and as such there is always the chance that some previously unstudied defect is present. However in the experience of these authors, contamination very often contains some portion of iron, and its recombination properties at such low concentrations make it highly likely that it is limiting the bulk lifetime.

III. IMPACT OF IRON IN COMPLETED SOLAR CELLS

The fundamental properties of iron discussed in the previous section predict that iron should spread quickly under standard production conditions and result in a severe impact on the recombination in the bulk of a solar cell. Here we provide experimental verification of this and demonstrate that the performance of solar cells contaminated with iron is well explained by the theory presented in the previous section.

The solar cells used in this study were produced on the DuPont-Innovalight 10MW pilot line facility. This line has

been shown to produce high efficiency screen-printed cells using both standard processing as well as Dupont™ Innovalight™ Silicon Ink selective emitter cells [9]. All samples were fabricated on standard industrial p-type CZ 156 mm pseudo square wafers. In both cases the fabrication sequence involved random pyramid texturing followed by SC2 cleaning (hyrogen peroxide, hydrochloric acid, and water). Prior to a $POCl_3$ emitter diffusion the wafers were cleaned in a sequence of buffered oxide etch (BOE), SC2, BOE, de-ionized (DI) water rinsing and drying in a Semitool spin-rinse-dryer. The front surface of the samples was coated with a PECVD deposited SiN layer, optimised for high performance under encapsulation, which also acted as a hydrogen source during metal firing. Metal contacts were formed using standard screen printed Al and Ag pastes, fast firing (~1s at 810 °C) in a Despatch belt furnace and laser edge isolation. IV characteristic of the fabricated solar cells were measured on a HALM flash IV tester. All cell lots run on the line were accompanied by test structures used to monitor minority carrier lifetime. These test structures were processed together with the lot wafers up to the metallisation step. At this point, the rear surface of the test structures was passivated with a second SiN deposition and the samples were fired alongside the cells.

During the operation of this line over the last 5 years there were instances of contamination that were detected. In all cases it was found that iron was the dominant defect and that the impurity was always extrinsically introduced through contact with contaminated surfaces. Examples from these batches are presented here to demonstrate the impact of iron on standard solar cell performance and how an extrinsic contamination source can be quickly identified.

A. Iron contaminated solar cells

To demonstrate the impact of iron contamination on the 1-Sun IV performance of screen printed solar cells we selected from three sample sets with varying contamination levels. These cells were characterised immediately after production (Ini), after 48 hours of light soaking (LS) and after recovery in the dark (Rec). The initial light-soaking step was intended to activate both BO complexes in the silicon as well as to convert any FeB pairs into interstitial Fe_i. By allowing at least 2 hours recovery in the dark, the vast majority of Fe_i atoms re-paired with B, greatly reducing its impact on the cell performance. It should be noted that if the only defect of interest is iron then it is possible to use a much shorter light soak step to activate the interstitial iron. The results here were taken from the routine characterisation procedure at DuPont in which light-induced degradation of the cells is monitored.

The IV characteristics for three sample sets after each stage are summarised in Fig. 2. The data is shown as an absolute change relative to the starting 1-Sun IV values. The "No Fe" sample set is considered to not contain significant levels of mobile iron. In this case the light soak step created a decrease in efficiency (-0.3%abs) which was not recovered after subsequent storage in the dark. The remaining two sets contained moderate and heavy levels of iron contamination. In both cases the light soak step caused a drop in efficiency which then partially recovered after storage in the dark.

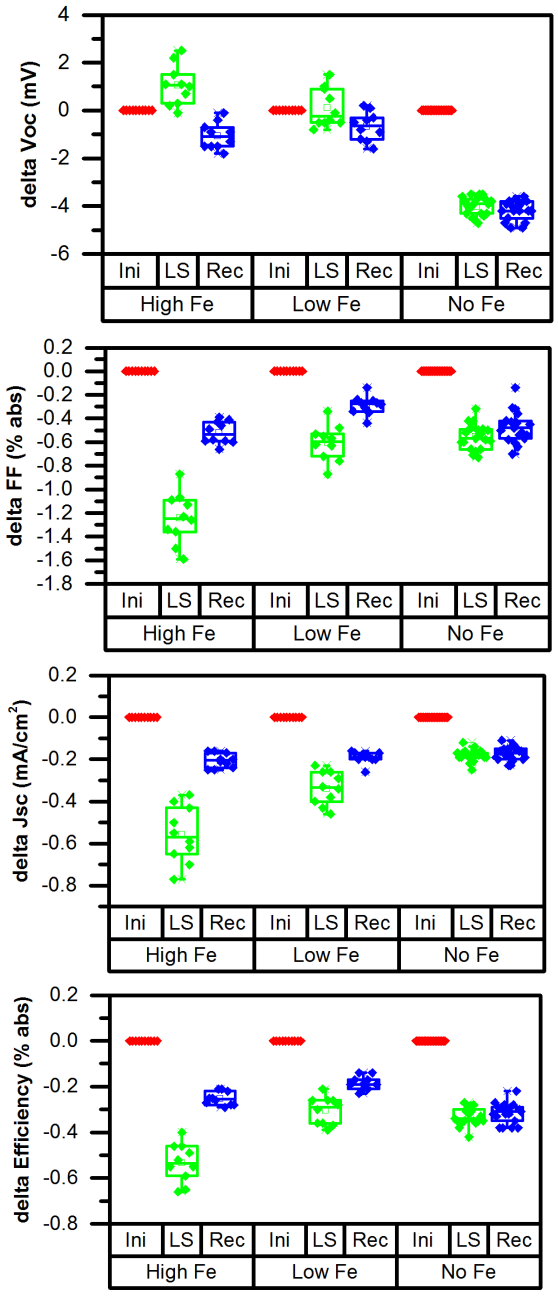

Fig. 2. Impact of illumination and dark recovery on the 1-Sun IV parameters of three sets of solar cells that contain various levels of iron contamination.

The changes in the IV characteristics of the cells above can be explained by the formation of both BO complexes as well as the transition between FeB and Fe_i^+ defects within the wafer bulk. In the case of the samples with no iron

contamination, the reduction in efficiency is attributed solely to the formation of BO complexes. Storage in the dark does not anneal out these defects and the loss in the different parameters remains permanent at the last stage of characterisation. On the other hand, the samples contaminated with interstitial iron were expected to have a bulk lifetime that was much more dependent on the minority carrier concentration. At the operating point that corresponded to Voc the lifetime was actually improved resulting in an increase in voltage. At the Jsc operating point the reverse occurred, at those low levels of excess minority carrier concentration (~10^{12} cm^{-3}) the interstitial iron created much higher recombination leading to a greatly reduced current. The transition between these two points was highly non-linear, resulting in a reduction in FF. Further characteristics of this FF reduction are discussed below. It is worth noting that the illumination provided by a flash tester is unlikely to fully convert all of the iron into the more detrimental interstitial form. This results in a difference in the measured IV performance compared to how the cells would perform either under a continuous light IV tester or under real conditions in the field.

B. Iron contamination – bulk quality recovery time constant

The transition between the different bulk recombination properties was further illustrated by monitoring the IV parameters of an iron contaminated cell while it recovered in the dark. This was done by placing the cell on the flash IV tester immediately after light soaking and measuring the IV data every 5 minutes. The changing value of each of the parameters was then fit using a simple exponential equation. It was found that all IV parameters could be fit with the same equation, an example of this fit is shown in Fig. 3. The extracted value for the time constant in this case was 3000s, which was quite consistent with the association constant calculated for this type of substrate using Eq. 2.

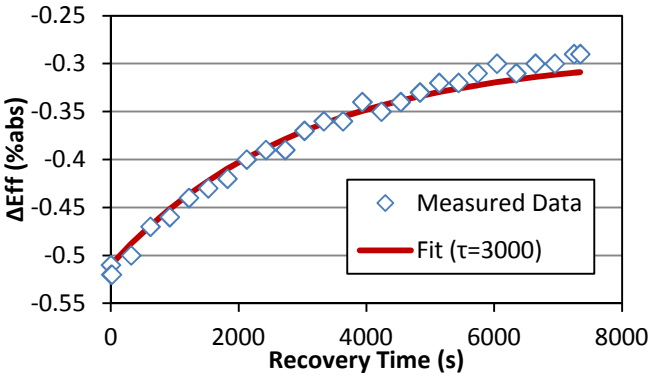

Fig. 3. The change in 1-Sun efficiency of an iron contaminated solar cell, as a function of time after removal from light soaking.

C. Characterising Fe contamination

The iron contaminated cells presented in the previous section showed a severely degraded FF. Such a reduction in FF due to bulk defects with strongly asymmetric SRH recombination properties has been demonstrated in the literature [1] and is certainly expected for significant levels of iron contamination. There are numerous techniques to confirm that a reduced FF is caused by recombination (e.g. dark-IV, Suns-Voc). Here we use dark-IV measurements with local ideality factor versus voltage (m-V) curves to confirm that a changing diode recombination current is responsible for this drop.

An illustration of the impact of an asymmetric SRH recombination source on the FF of a solar cell was demonstrated in the dark-IV curves of an iron contaminated sample measured every 30 minutes after the light soak step (the same sample shown in Fig. 3. above). The plot of the m-V characteristics extracted for these curves, shown in Fig. 4, exhibited a changing ideality factor at the voltages critical for determining the FF. At the start of recovery, when iron in the bulk of the sample was predominantly interstitial, the extreme asymmetry of the recombination resulted in a local ideality factor of ~1.45 at the max power point voltage. As the sample started to recover in the dark, the pairing of Fe and B resulted in progressive reduction of the ideality factor, which dropped to ~ 1.3 after 2 hours of dark storage. This change in ideality factor corresponded in an absolute decrease in FF of 0.6%.

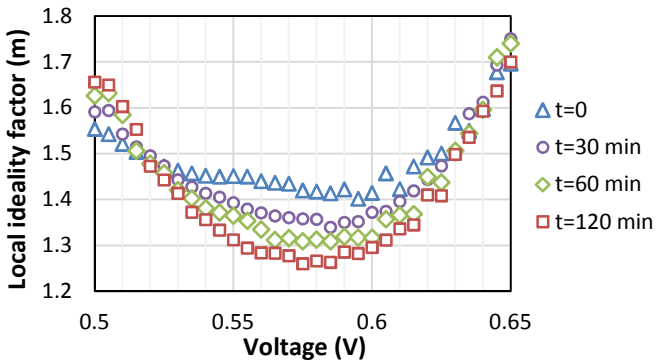

Fig. 4. Local ideality factor versus voltage for an iron contaminated solar cell after various wait times since a light soak at 1-Sun.

The impact of specific SRH defects on the recombination current of a solar cell can be further investigated using cell simulations. This technique can be useful for validating that a particular defect may be the root cause of a problem as well as to predict how other cell architectures would respond to such a contamination. Using the known recombination properties of various defects it is also possible to estimate how detrimental various impurities are to a new cell technology. This information can be particularly useful when assessing candidate chemicals to use in cell processing.

To simulate the contaminated solar cell from Fig. 4. we used Quokka 2.2 [10], a simulation package freely available at www.pvlighthouse.com.au. The settings used to define the simulation with an iron contaminated bulk were created using the settings file generator [11]. To create dark IV curves the simulation was set to solve the IV curve for the case of no generation. The unit cell was defined in 2D with a width of 1100 um, a top contact width of 50 µm and a full area rear contact. The rear surface boundary was defined as a 30 Ω/□ conductive layer with a recombination current defined by an effective surface recombination velocity of 300 cm/s. The front boundary was a 70 Ω/□ conductive layer with recombination defined by the J_0 model with 100 fA/cm^2 in the non-contact regions and 300 fA/cm^2 at the metal interface. Other parasitic loss mechanisms were approximated using external circuit elements: (1) a diode with m = 2 and J_{0ext} =1.4 x 10^{-8} A/cm^2, (2) a 3.3 kΩ·cm^2 shunt resistor and (3) a 0.25 Ω·cm^2 series resistor. The background bulk lifetime (τ_{bac}) was then varied between 200 µs and 500 µs as was the concentration of either Fe_i or FeB to achieve the best fit to the data measured on the iron contaminated sample. The final results, shown in Fig. 5, used τ_{bac} = 300 µs and an iron concentration of 7 x 10^{10} cm^{-3}.

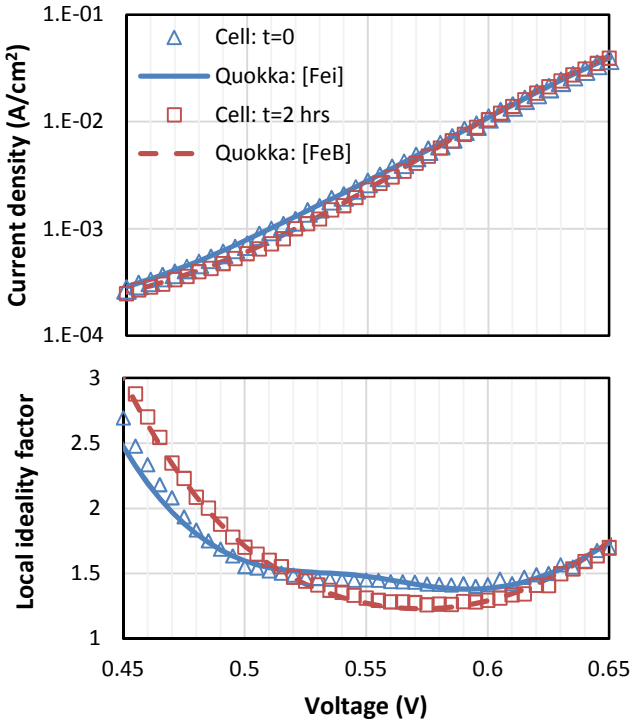

Fig. 5. Dark current density (top) and local ideality factor (bottom) versus voltage for an iron contaminated solar cell measured (blue triangles) immediately after a 1-Sun light soak and (red squares) after 2 hours recovery in the dark. The results of a Quokka simulation are also shown as (blue solid line) [Fe_i]=7x10^{10} cm^{-3} and (red dashed line) [FeB]=7x10^{10} cm^{-3}

By changing between these two bulk defects (and changing no other parameters) the simulation tool was able to explain the shift observed in the dark IV curves. It should be noted that in this simulation we neglected the impact of any asymmetric recombination caused by BO pairs and instead lumped their impact into the background bulk lifetime.

IV. Sources of Fe Contamination in Silicon Solar Cell Production

In production environments there are many opportunities for iron to be transferred from the production line onto the surface of silicon wafers from where it can diffuse into the bulk during subsequent thermal processes. The previous section demonstrated the negative impact that this has on solar cells and how iron presence can be detected on finished cells. To mitigate the problem in a process line it is necessary to locate the source of contamination and understand how it has spread through the production environment. The technique used to achieve this here was to run test wafers through isolated sections of the cell line and then use photoluminescence (PL) imaging to identify the root cause. In doing so various contamination sources and transfer mechanisms were identified and subsequently removed. These examples demonstrate how contamination may behave in similar production environments.

In the first example the samples were processed on a three lane inline iso-texture tool. After this processing the wafers were cleaned, rinsed and spin-dried before a standard $POCl_3$ emitter process followed by double sided PECVD nitride and firing. PL images of the samples, examples shown in Fig. 6, identified a region of poor lifetime on two out of every three wafers. Subsequent lifetime testing detected significant concentration of iron in this region. The source of the contamination was identified as a slight defect on the exit ramp of the tool in which one lane had a slight raised bump in the plastic which over time had worn away the surface coating and exposed the underlying plastic. The contamination from one out of every three wafers was then transferred (presumably during diffusion) onto the adjacent wafer. It is interesting that in this case, despite the locally high levels of iron detected, the contamination did not spread further. Repairs to the exit ramp of the tool removed this contamination source from the line.

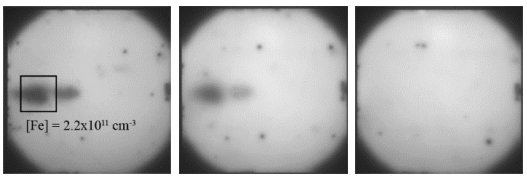

Fig. 6. 1-Sun PL images of test structures processed in an inline isotexture bench.

Another example of iron contamination occurred when some wafers were weighed on a scale with a circular metal sample holder. This measurement was made before and after

the texturing process as a form of process control (although it was not originally intended that the silicon come in direct contact with the metal). PL images of these wafers (Fig. 7) revealed immediately that a contamination event had occurred and the distinct shape allowed for easy identification of the source. The $POCl_3$ based emitter formation process provided a high temperature step in which contamination was able to spread both within the contaminated wafer (wafer 1) as well as to adjacent wafers (wafers 2 through 5), which did not come in a direct contact with a metal part. The adjacent wafers appear to have been cross contaminated during the high temperature diffusion process. Lifetime testing to measure the iron concentration yielded [Fe] = $8.8x10^{11}$ cm^{-3} on wafer 1 and [Fe] = $7.7x10^{10}$ cm^{-3} for wafer 5 on the right. This contamination source was removed by avoiding future contact with the metal scale, replacing all baffle wafers in the tube furnace and cleaning the furnace (and quartz boats) with TCA.

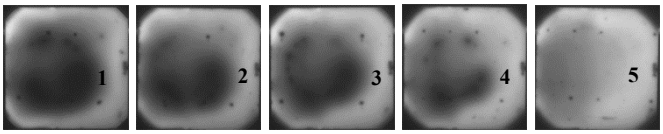

Fig. 7. Example of contamination spread between adjacent wafers during a $POCl_3$ diffusion process. Presented as 1-Sun PL images.

Wet chemistry steps also provide a very effective mechanism to redistribute contamination, particularly laterally across a surface [12]. A particular example that this is occurring can be circular patterns (Fig. 8) which - in this case - resulted from the subsequent spin-rinse-drying process.

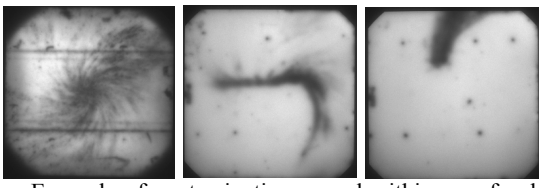
Fig. 8. Example of contamination spread within a wafer during a spin-rinse-dry process. Presented as 1-Sun PL images.

It is worth noting that prior to the introduction of a specific contamination source the cleaning processes used in the above examples had been shown to be capable of consistently supporting very high lifetimes [13]. With the general industry push to reduce costs it is likely that the various cleaning techniques used to mass produce solar cells will be pushed to a bare minimum. To support the use of this while maintaining solar cell efficiency it will be necessary to ensure extrinsic contamination is avoided.

V. Conclusion

The nature of iron contamination of silicon solar cells has been presented both theoretically and experimentally. It has been shown that the performance of iron contaminated solar cells can be explained by the well-understood fundamental properties of mobile iron in silicon. The transient nature of the efficiency degradation and recovery due to iron was demonstrated. Characterisation of iron contaminated cells further confirmed the impact of bulk SRH defects on solar cell performance and it was demonstrated that these effects can be accurately reproduced by solar cell simulations. Finally, the paper presented a series of examples of contamination that occurred in a production style environment. These examples demonstrated the propensity for iron to move from production equipment and process chemicals onto a wafer and for subsequent processing to further distribute this contamination.

VI. References

[1] D. Macdonald and A. Cuevas, "Reduced fill factors in multicrystalline silicon solar cells due to injection-level dependent bulk recombination lifetimes", *Progress in Photovoltaics: Research Applications*, **8**, pp. 363-375, (2000)

[2] M.C. Schubert, J. Schon, B. Michl, A. Abdollahinia, W. Warta, "Modeling distribution and impact of efficiency limiting metallic impurities in silicon solar cells", in *38th IEEE Photovoltaic Specialist Conference*, (2012)

[3] R. Kvande, L. J. Geerligs, G. Coletti, L. Arnberg, M. Di Sabatino, E. J. Øvrelid, and C. C. Swanson, "Distribution of iron in multicrystalline silicon ingots", *Journal of Applied Physics*, **104**, 064905, (2008)

[4] A.A. Istratov, H. Hieslmair, E.R. Weber, "Iron contamination in silicon technology", *Applied Physics A,* **70**, 489–534 (2000)

[5] D. H. Macdonald, L. J. Geerligs, and A. Azzizi, "Iron detection in crystalline silicon by carrier lifetime measurements for arbitrary injection and doping", *Journal of Applied Physics,* **95**, 1021 (2004)

[6] A.A. Istratov, H. Hieslmair, E.R. Weber, "Iron and its complexes in silicon", *Applied Physics A,* **69**, 13–44 (1999)

[7] D. Macdonald, T. Roth, P.N.K. Deenapanray, T. Trupke and R.A. Bardos, "Doping dependence of the carrier lifetime crossover point upon dissociation of iron-boron pairs in crystalline silicon" Applied Physics Letters. **89**, 142107 (2006)

[8] D. Macdonald, T. Roth, P.N.K. Deenapanray, K. Bothe, P. Pohl, and J. Schmidt, "Formation rates of iron-acceptor pairs in crystalline silicon", *Journal of Applied Physics,* **98**, 083509 (2005)

[9] G. Scardera, A. Meisel, K.R. Mikeska, A.F. Carroll, M.Z. Burrows, D. Poplavskyy, M. Abbott, F. Lemmi, H. Antoniadis, "High Efficiency Phosphorus Emitters for Industrial Solar Cells: Comparing Advanced Homogeneous Emitter Cells and Selective Emitters using Si Ink Technology", in *27th EU Photovoltaic Specialist Conference*, (2012)

[10] A. Fell, "A free and fast 3D/2D solar cell simulator featuring conductive boundary and quasi-neutrality approximations," *IEEE Transactions on Electron Devices,* **60** (2), pp. 733–738, (2012)

[11] http://www.pvlighthouse.com.au/Resources/quokka2/quokka2 settings file generator.aspx

[12] S. Baker-Finch, K.R. McIntosh, "Photoluminescence Imaging Diagnosis of Particulate Iron Contamination Derived From HF Dip and Thermal Oxidation," *IEEE Journal of Photovoltaics*, **1**, no.1, pp.66, 71, (2011)

[13] H. Antoniadis,"Silicon ink high efficiency solar cells", in *34th IEEE Photovoltaic Specialists Conference* (2009)